NUMERICAL INVESTIGATION OF IN-CYLINDER FUEL ATOMIZATION AND MIXING FOR A GDI ENGINE

2 AUTHORS:

Ajay Mandyam Rangarajan
RWTH Aachen University
2 PUBLICATIONS **1** CITATION
SEE PROFILE

R. Banerjee
Indian Institute of Technology Hyderabad
25 PUBLICATIONS **67** CITATIONS
SEE PROFILE

Proceedings of the 22th National and 11th International ISHMT-ASME Heat and Mass Transfer Conference December 28-31, 2013, IIT Kharagpur, India

HMTC1300405

NUMERICAL INVESTIGATION OF IN-CYLINDER FUEL ATOMIZATION AND MIXING FOR A GDI ENGINE

Ajay M Rangarajan
Indian Institute of Technology Hyderabad
Hyderabad, AP, 502205
India
me09b003@iith.ac.in

R. Banerjee
Indian Institute of Technology Hyderabad
Hyderabad, AP, 502205
India
rajabanerjee@iith.ac.in

ABSTRACT

Gasoline Direct Injection (GDI) engines have been shown to have better fuel economy, transient response and cold-start hydrocarbon emissions. Additionally they have lower NOx emissions when operated under lean conditions. However, controlling charge stratification under various load conditions is a major challenge in GDI engines. In the present study a numerical simulations have been performed to understand factors affecting air/fuel mixture preparation under various engine operating conditions. Fuel spray atomization was studied using the two-way coupled Eulerian-Lagrangian approach. Momentum, energy and species equations were solved for the continuous gas phase. The droplet life history was tracked using the Lagrangian approach. Parameters like fuel injection time, fuel mass flow rate and engine speed was varied to determine their effect on air/fuel mixture preparation inside the cylinder.

NOMENCLATURE

A	Area (m^2)
B	Spalding number
C_d	Coefficient of discharge
Cp	Constant pressure specific heat (kJ/kgK)
d_o	Injector inner diameter (m)
D_p	Droplet diameter (m)
F_s	Surface force (N)
F_b	Body force (N)
g	Acceleration due to gravity (m/s^2)
h_e	Heat transfer coefficient (WK/m^2)
h_{eff}	Effective latent heat of evaporation (J/kg)
k	Thermal conductivity (WK/m)
$\dot{m}$	Mass flow rate (kg/s)
n	Number density (m^{-3})
Nu	Nusselt number
Δp	Pressure gradient (Pa/m)
r	Position vector
Δt	Time step size (s)
t	Time (s)
T	Temperature (K)
u_f	Axial velocity film velocity (m/s)
v	Velocity (m/s)
V	Volume (m^3)
V_c	Control volume (m^3)

Greek symbols

ρ	Desnity (k/m^3)
δ	Dirac delta function
δ_o	Film thickness (m)

Subscript

f	Film
p	Droplet
s	Droplet surface
π	Droplet parcel

INTRODUCTION

Vehicle manufacturers are turning to advanced engine technologies to improve efficiency and meet strict fuel economy and emissions requirements. Among the many technologies and strategies proposed by researchers worldwide, a direct-injection (DI), four-stroke SI engine, that minimizes the throttling to control the load, seem to be a promising candidate for achieving this. First of all, DI's charge cooling through in-cylinder injection helps in preventing knocking and therefore allows higher compression ratios and higher turbo-charging than Port Fuel Injection (PFI) engines [1], [2]. Also, downsized homogeneous-charged gasoline direct injected (GDI) engines will lead to fuel savings compared to current production PFI gasoline engine. Moreover, in this class of engines, the power output is controlled by varying the amount of fuel that is injected into the cylinder like diesel engine. The inducted air is less throttled thus minimizing the negative work of the pumping loop of the cycle. Furthermore, by means of an adequate design of the combustion chamber configuration and fluid-dynamics, overall lean-operation may be achieved, thus yielding an enhanced BSFC and lower NOx emissions. While the above mentioned benefits are important, the GDI fuel delivery optimization complexity is significantly higher than PFI engines. GDI engines must meet proper fuel vaporization and air/fuel mixing inside the cylinder. This is achieved by a higher injection pressure of the fuel, which results in atomized fuel droplets of much smaller diameter and by a careful optimization of the combustion chamber design and of the injection timing.

Several research groups are using various experimental and numerical techniques to study different aspects of GDI engine operations [3]. Bessler et al [4] studied NO formation using Laser Induced Fluorescence (LIF) technique in an engine with optical access. Zhao et al [5] studied the effect of hydrogen blending on particulate emission and combustion performance in a GDI engine. Higher hydrogen content made the combustion more stable and faster. Zigan et al [6] used a variety of optical techniques to evaluate the structure of a piezoelectric hollow cone fuel injector. Chen et al [7] studied the air/fuel mixture preparation of different ethanol/gasoline blends in an engine with optical access. Pyari et al [8] studied fuel spray characteristics from common rail multi-hole injectors using high speed imaging under non-reactive conditions.

Most major numerical investigation use Lagrangian approach to track the liquid droplet time-history. Assanis et al [9] implemented a low pressure spray breakup model in a multidimensional code and compared its performance with respect to the TAB model of O'Rourke and Amsden [10]. Takagi et al [11] studied the effect of cone angle of hollow cone swirl injector due to variations in the ambient pressure. Goryntsev et al [12] used Large Eddy Simulation (LES) for the continuous phase to determine the effect of cycle-to-cycle variation in velocity profile and subsequently its effect of air/fuel mixture preparation. Costa et al [13] reported results of numerical optimization analyses aimed at increasing the energetic efficiency of a GDI engine equipped with a high pressure multi-hole injector under both single and double injection events.

In the present study, Eulerian-Lagrangian approach was used to study the effect of different engine operating conditions on air/fuel mixture preparation under late injection conditions. Three different spray breakup models for a pressure swirl injector were initially evaluated with respect to experimental results from open literature. This injector was then used to study the air/fuel mixture preparation in a realistic 3D engine geometry. All simulations in this study were executed using the commercial CFD solver STAR-CCM+ v 7.4

MATHEMATICAL FORMULATION

Eulerian-Lagrangian approach was used to solve the governing equations in this study. The droplet trajectory is determined by integrating the forces acting on the particle. The net force acting on the droplet can be expressed as

$$m_p \frac{d\vec{v}_p}{dt} = \vec{F}_s + \vec{F}_b \tag{1}$$

The surface and body forces is expressed as,

$$\vec{F}_s = \frac{1}{2} C_d \rho A_p |\vec{v}_s| \vec{v}_s$$
$$\vec{F}_b = m_p \vec{g} \tag{2}$$

Slip velocity is defined as the difference in the velocities between the dispersed phase particles and the continuous phase. The droplets are assumed to have a low Biot number and therefore the temperature is assumed to be uniform. Energy balance across the droplet gives its temperature in the form,

$$m_p Cp \frac{dT_p}{dt} = f h_e A_s (T - T_p) + \dot{m}_p h_{eff} \tag{3}$$

The heat transfer coefficient is determined based on Ranz-Marshall correlation [14] and mass transfer correction, *f*, is determined using El Wakil et al [15] formulation. Due to the elevated temperature condition in the engine, heat transfer limited evaporation is considered, where the evaporation rate is given as,

$$\frac{dm_p}{dt} = -\frac{k\mathrm{Nu}_p}{CpD_p} A_s \ln(1+B) \tag{4}$$

As a two way coupling was assumed, mass, momentum and energy transfer from the dispersed phase to the continuous phase was modelled by incorporating source terms in the continuity, momentum, energy and species equations of the continuous phase and they are of the form:

$$S_m = -\frac{1}{\Delta t} \sum \left(\int_t^{t+\Delta t} \int_{V_c} \delta(r - r_\pi) n_\pi \dot{m}_p dV dt \right)$$

$$S_v = -\frac{1}{\Delta t} \sum \left(\int_t^{t+\Delta t} \int_{V_c} \delta(r - r_\pi) n_\pi (F_s + \dot{m}_p v_p) dV dt \right)$$

$$S_E = -\frac{1}{\Delta t} \sum \left(\int_t^{t+\Delta t} \int_{V_c} \delta(r - r_\pi) n_\pi \left(Q_t + F_s v_p + \frac{1}{2}\dot{m}_p v_p^2 + \dot{m}_p h\right) dV dt \right) \tag{5}$$

$$S_{mi} = -\frac{1}{\Delta t} \sum \left(\int_t^{t+\Delta t} \int_{V_c} \delta(r - r_\pi) n_\pi \dot{m}_{pi} dV dt \right)$$

As the pressure swirl injector produces a hollow cone spray, LISA spray breakup model as proposed by Senecal et al [16] was used to model the primary jet breakup. The initial liquid sheet thickness, δ_o, of the liquid jet emanating from the injector is given as

$$\dot{m}_f = \pi \rho u_f \delta_o (d_o - \delta_o) \tag{6}$$

It is assumed that the liquid film velocity is uniform along its circumference and is expressed as,

$$|v_f| = k_v \sqrt{\frac{2\Delta p}{\rho}},$$
$$\text{where} k_v = \max\left[0.7, \frac{4\dot{m}}{\pi d_o^2 \cos\theta} \sqrt{\frac{\rho}{2\Delta p}}\right] \tag{7}$$
$$\text{and} u_f = v_f \cos\theta$$

There are several secondary breakup models available with STAR-CCM+, which includes the TAB model proposed by O' Rourke and Amsden [10], KH-RT model by Beale and Reitz [17] and Reitz Diwakar model [18], [19]. All the three were evaluated and their comparison is reported in the Validation section of this paper.

VALIDATION

A large number of parameters affect fuel atomization characteristics, ex: injection pressure, ambient pressure and temperature, nozzle geometry, etc. Additionally, all spray models have large number of model parameters which are empirical in nature. Therefore, it is important to validate a particular fuel injection with experimental data. In the present study, validation of a pressure swirl injector inside a constant volume cylinder was performed. Spray penetration depth, which is defined as the axial distance of the liquid fuel from the injector exit, was used as the parameter for the validation study. The penetration depth from the CFD simulations were compared with experimental results as reported by Fontanesi et al [20].

To calculate the penetration depth, severak surfaces were created which were 2mm apart. The summation of volume

fraction of liquid fuel across these surfaces was saved as a function of time. The farthest plane from the injector with a volume fraction more than 0.02 was taken as the penetration length. The sensitivity of results towards the choice of value 0.02 was checked and found to be minimal. This volume fraction data from the different planes was then converted to penetration depth versus time.

Figure 1. shows the penetration depth time history from the three spray breakup models and compared with the experimental results from reference [20]. As can be seen from the figure, the Reitz-Diwakar model gives the best comparison with experimental results. The KHRT break-up model performs well in the later part of the spray but required a lower time step in certain portions of the simulation and was not a very suitable choice.

RESULTS AND DISCUSSION

In the present study, engine geometry as given in figure 2 was used for all the simulations. As effects of late injection strategy on air/fuel mixture preparation was investigated, it was assumed that both the inlet and exhaust valve of the cylinder was closed and only compression stroke was considered. Hence no exchange of charge to and from the engine volume was considered. Fuel was directly injected inside the cylinder volume and it was directed towards the piston bowl. The engine geometry and piston bowl geometry was approximated as given in [9]. Tables 1and 2 gives the details of the engine parameters and injector details used in this study.

The compression stroke was simulated using the moving mesh technique called 'Morpher' available in STAR-CCM+. This technique allows the bottom wall (the piston bowl) to move up with a specified velocity as determined from piston velocity calculations. The simulation of piston motion was run for a few cycles without any injection to establish the air flow conditions present in an engine. Once the air flow patterns were established, an injection was performed. A parametric variation of the injection time, injection length and also engine speed was carried out

Base Case Analysis

A base case was simulated to understand the time history of the fluid flow and mixing during the compression stroke of the engine. In this case the fuel was injected at 90^o BTDC and the injection length was 20^o of Crank Angles (CA). The engine RPM was maintained at 1500 rpm. Figure 3 shows the droplet time history, temperature profile, velocity vectors and equivalence ratio at three different crank angles.

As can be seen from the droplet particle trace, the droplets are injected towards the piston bowl. Due to the pressure swirl nature of the injector, the particles fan out after exiting the injector and occupy a fairly large volume of the available cylinder geometry. This aids in the evaporation process of the fuel. By 50^o BTDC only few droplet parcels are present and when the piston is at TDC, almost all droplets have evaporated. Though not very clear from the figure given here, some droplets get deposited on the piston walls and a film of liquid is formed.

When analyzing the velocity, temperature and equivalence ratio plots, it is observed that there is strong interaction of the flow with the piston bowl at around 50^o BTDC. Due to its shape, a strong tumble motion is observed as the flow is directed towards the central portion of the cylinder head. The spark plug is assumed to be located in this region and therefore a fuel rich condition will observed in this location. Temperature of the gas phase is reduced in the vicinity of the spray due to evaporative cooling. Charge cooling which in turn helps in increasing the volumetric efficiency due to this mechanism is consistent with the stated advantage of a GDI engine. The vapor follows the carrier gas velocity profile and therefore its distribution is very similar to the velocity and temperature profiles of the gas phase. A clear charge stratification is observed at 10^o BTDC when the spark event happens. Fuel rich conditions are present at this location and the equivalence ratio reduces significantly near the piston walls. In some regions the equivalence ratio is significantly larger particularly near the cylinder walls indicating that fuel film may be present in these regions.

Effect of Injection Timing

In this parametric study the start of injection was changed. The following injection time was investigated: 160^o, 90^o, 45^o and 20^o BTDC. Injection length and engine rpm was kept same as the base case. Figure 4 (a) shows the vapour mass fraction contours along the spark plug cross-section at 10^o BTDC and Figure 4 (b) shows the time history of the vapour mass fraction at the vicinity of the spark plug. As can be seen from the figures, the vapour mass fraction for the 160^o case very homogenized as the vapour gets sufficient time to mix with the ambient air. Therefore the mass fraction rise near the spark plug is relatively low and continuously rising with time. As injection time is successively retarded, the vapour mass fraction distribution becomes more stratified and the time history plot shows a rapid increase of vapour near the spark plug. However, in case of 20^o start of injection, the vapour mass fraction is very low because the simulation stopped after only 20 CA as the piston reached TDC and therefore injection was incomplete.

Effect of Injection Length

In this case the length of fuel injection was changed from 10^o CA to 25^o CA with an increment of 5^o. With increase in injection length, the mass flowrate of the fuel emanating from the injector decreases. Therefore, it is expected that the penetration depth of the fuel will also consequently decrease. This will also result in less impingement of fuel on the piston and cylinder wall. Effects of fuel impingement is clearly observed in the cross-section vapour contour plots of Figure 5 (a). For 10^o and 15^o CA, regions of large vapour mass fraction is seen close certain regions of the wall. However, when injection length is further increased, these regions no longer appear in the cross-section. The cross-sectional plot for 25^o CA is very homogenized. This maybe because the velocity of the fuel droplets is low when the injection length is increased. Therefore, the surrounding air tends to entrain larger amount of droplets, which in turn results in more uniform air/fuel mixture preparation. However, when the vapour mass fraction time history is investigated at the spark location, all the plots are similar other than the plot from 10^o CA. The early rise in the vapour mass fraction for 10^o CA can be attributed to the higher mass flowrate of the injected fuel. For other injection lengths, the fuel velocity seems to have fallen beyond a certain threshold and therefore vapour mass fraction rise is unaffected by any change in injection length.

Effect of Engine RPM

Effect of engine RPM was expected to have a strong influence on air/fuel mixture preparation because the in-cylinder charge motion is strongly influenced by engine speed. Four different engine speeds were simulated starting from 1000 RPM, which is the typical speed at ideal and it was increased to a maximum of 2500 RPM, which corresponds to cruising speed. Higher engine loads that is typical during high acceleration was not modeled because is such cases the injection event is much earlier; typically during the intake stroke. As can be seen from Figure 6, air/fuel stratification becomes more prominent at

higher engine RPM. This is because, the effect of tumble due to piston bowl geometry becomes stronger at higher engine RPM, which in turn entrains larger amount of fuel droplets. Due to this larger entrainment, the fuel droplets and consequently its vapour is confined to a more limited volume within the cylinder. The time history mass of the vapour fraction near the spark plug continuously increases for 1000RPM case and this is because the air/fuel mixture is fairly homogeneous. In all the other cases, the mass fraction initially increases and the values reach a peak value at a certain CA. The vapour mass fraction then decreases on further compression. The maximum value of the vapour mass fraction and its rate of decrease from its peak is influenced by the in-cylinder charge motion.

CONCLUSION

In this study, influence of fuel injection and engine speed was numerically studied on air/fuel mixture preparation for a GDI engine. It was seen that after fuel was injected within the engine, the fuel droplets are entrained along with the surrounding air. This entrainment is influenced not only by piston bowl geometry but also with the engine operating parameters. Charge stratification is not always achieved. If the fuel droplets have large residence time after injection, charge homogenization tends to occur. However, at higher engine speed, charge flow due to tumble within the cylinder helps in stratified mixture preparation.

REFERENCES

[1] R. Rotondi and G. Bella, "Gasoline direct injection spray simulation," *International Journal of Thermal Sciences*, vol. 45, no. 2, pp. 168–179, 2006.

[2] F. Zhao, M.-C. Lai, and D. . Harrington, "Automotive spark-ignited direct-injection gasoline engines," Progress in Energy and Combustion Science, vol. 25, no. 5, pp. 437–562, 1999.

[3] M. C. Drake and D. C. Haworth, "Advanced gasoline engine development using optical diagnostics and numerical modeling," *Proceedings of the Combustion Institute*, vol. 31, no. 1, pp. 99–124, 2007.

[4] W. G. Bessler, M. Hofmann, F. Zimmermann, G. Suck, J. Jakobs, S. Nicklitzsch, T. Lee, J. Wolfrum, and C. Schulz, "Quantitative in-cylinder NO-LIF imaging in a realistic gasoline engine with spray-guided direct injection," *Proceedings of the Combustion Institute*, vol. 30, no. 2, pp. 2667–2674, Jan. 2005.

[5] H. Zhao, R. Stone, and L. Zhou, "Analysis of the particulate emissions and combustion performance of a direct injection spark ignition engine using hydrogen and gasoline mixtures," *International Journal of Hydrogen Energy*, vol. 35, no. 10, pp. 4676–4686, May 2010.

[6] L. Zigan, I. Schmitz, A. Flügel, M. Wensing, and A. Leipertz, "Structure of evaporating single- and multicomponent fuel sprays for 2nd generation gasoline direct injection," *Fuel*, vol. 90, no. 1, pp. 348–363, Jan. 2011.

[7] L. Chen, R. Stone, and D. Richardson, "A study of mixture preparation and PM emissions using a direct injection engine fuelled with stoichiometric gasoline/ethanol blends," *Fuel*, vol. 96, no. null, pp. 120–130, Jun. 2012.

[8] R. Payri, A. García, V. Domenech, R. Durrett, and A. H. Plazas, "An experimental study of gasoline effects on injection rate, momentum flux and spray characteristics using a common rail diesel injection system," *Fuel*, vol. 97, no. null, pp. 390–399, Jul. 2012.

[9] D. N. Assanis, S. J. Hong, A. Nishimura, G. Papageorgakis, and B. Vanzieleghem, "Studies of Spray Breakup and Mixture Stratification in a Gasoline Direct Injection Engine Using KIVA-3V," *Journal of Engineering for Gas Turbines and Power*, vol. 122, no. 3, p. 485, Jul. 2000.

[10] P. J. O'Rourke and A. . Amsden, "The TAB Method for Numerical Calculation of Spray Droplet Breakup," in *SAE Paper 872089*, 1987.

[11] M. Takagi and Y. Moriyoshi, "Modelling of a hollow-cone spray at different ambient pressures," *International Journal of Engine Research*, vol. 5, no. 1, pp. 39–52, Jan. 2004.

[12] D. Goryntsev, A. Sadiki, M. Klein, and J. Janicka, "Large eddy simulation based analysis of the effects of cycle-to-cycle variations on air–fuel mixing in realistic DISI IC-engines," *Proceedings of the Combustion Institute*, vol. 32, no. 2, pp. 2759–2766, 2009.

[13] M. Costa, U. Sorge, and L. Allocca, "Increasing energy efficiency of a gasoline direct injection engine through optimal synchronization of single or double injection strategies," *Energy Conversion and Management*, vol. 60, no. null, pp. 77–86, Aug. 2012.

[14] W. E. Ranz and W. R. Marshall, "Evaporation from Drops, Part-1," *Chemical Engineering Progress*, vol. 48, pp. 141–146, 1952.

[15] M. M. El Wakil, O. A. Ueyhara, and P. S. Myers, "A theoretical investigation of the heating-up period of injected fuel droplets vaporizing in air," 1954.

[16] P. . Senecal, D. . Schmidt, I. Nouar, C. . Rutland, R. . Reitz, and M. . Corradini, "Modeling high-speed viscous liquid sheet atomization," *International Journal of Multiphase Flow*, pp. 1073–1097, 1999.

[17] J. C. Beale and R. D. Reitz, "Modeling Spray Atomization with the Kelvin-Helmholtz/Rayleigh-Taylor Hybrid Model," *Atomization and Sprays*, vol. 9, no. 6, 1999.

[18] R. D. Reitz and R. Diwakar, "Effect of drop breakup on fuel sprays," in *SAE Paper 860469*, 1986.

[19] R. D. Reitz and R. Diwakar, "Structure of high-pressure fuel sprays," in *SAE Paper 870598*, 1987.

[20] S. Fontanesi, V. Gagliardi, S. Malaguti, G. Valentino, and M. Auriemma, "Detailed Experimental and Numerical Investigation of the Spray Structure in a GDI High-Pressure Swirl Injector," in *Paper ID ICLASS06-189, ICLASS-2006*, 2006.

Table 1. ENGINE PARAMETERS

Parameters	Value
Ambient pressure	0.1 MPa
Engine cylinder temperature at BDC	700 K
Injection temperature	300 K
Stroke length	0.078 m
Rod to crank ratio	1.64
Compression ratio	9

Table 2. INJECTOR PARAMETERS

Parameter	Value
Injector type	Pressure swirl injector
Injection pressure	10 MPa
Inner cone angle	62 deg
Outer cone angle	72 deg
Injector diameter	5e-4 m

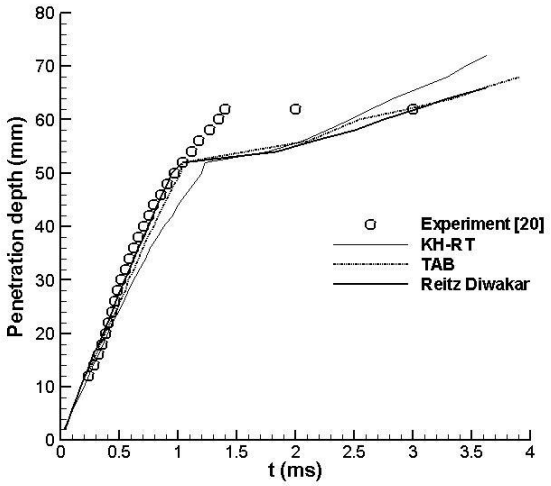

Figure 1. COMPARISON OF PENETRATION DEPTH

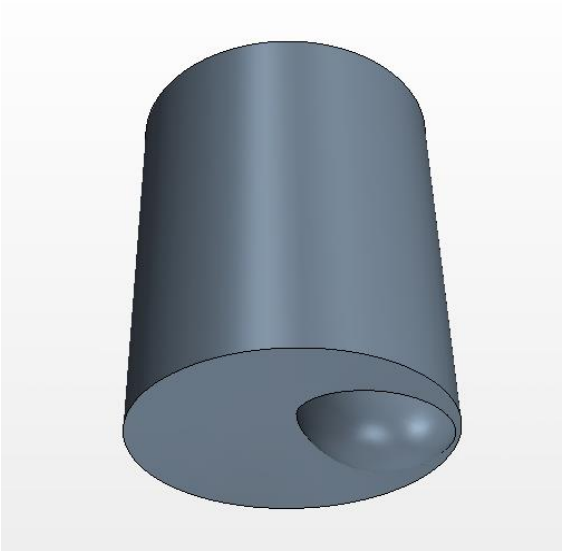

Figure 2. PISTON BOWL GEOMETRY

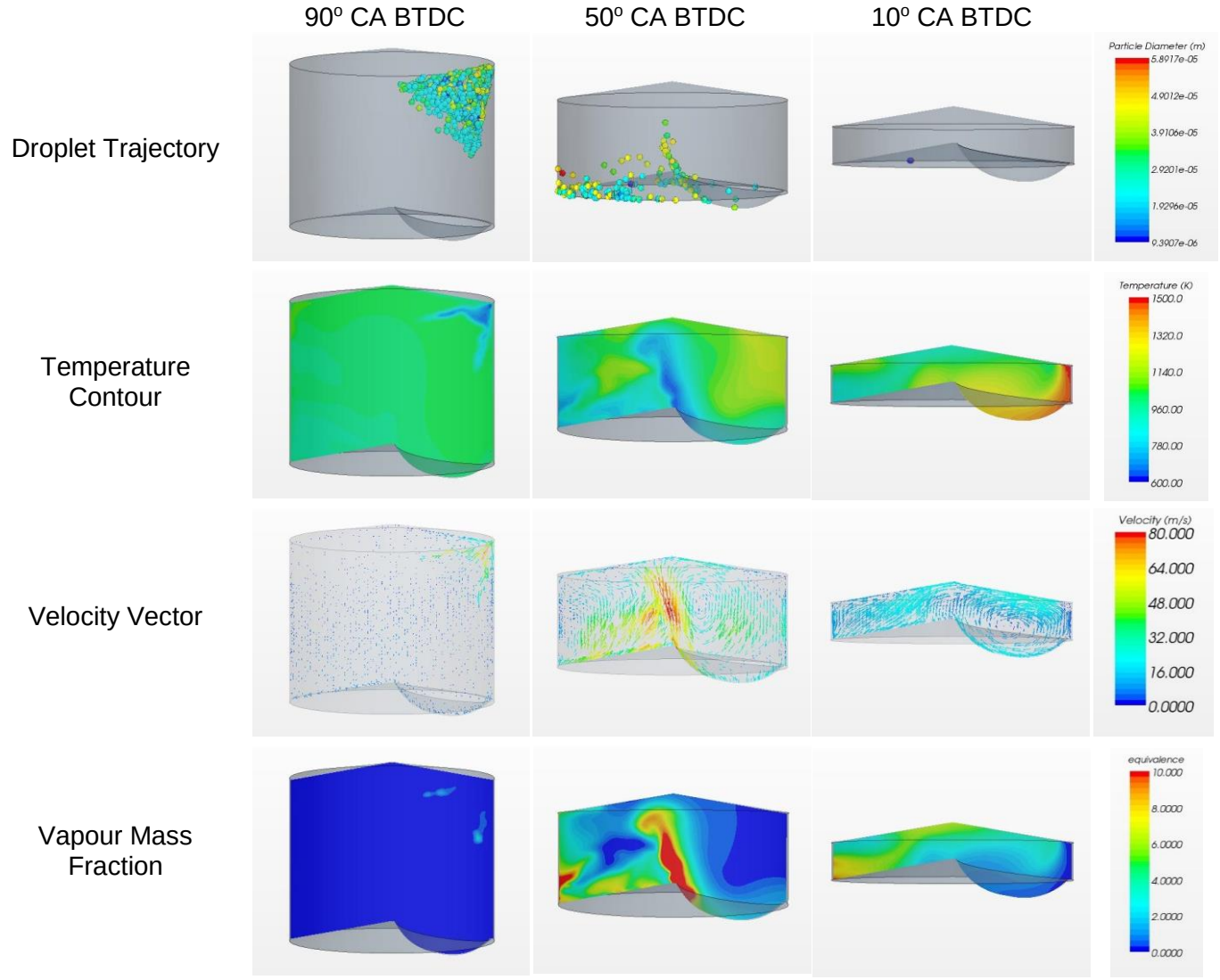

Figure 3. RESULTS FROM BASE CASE AT DIFFERENT CRANK ANGLES

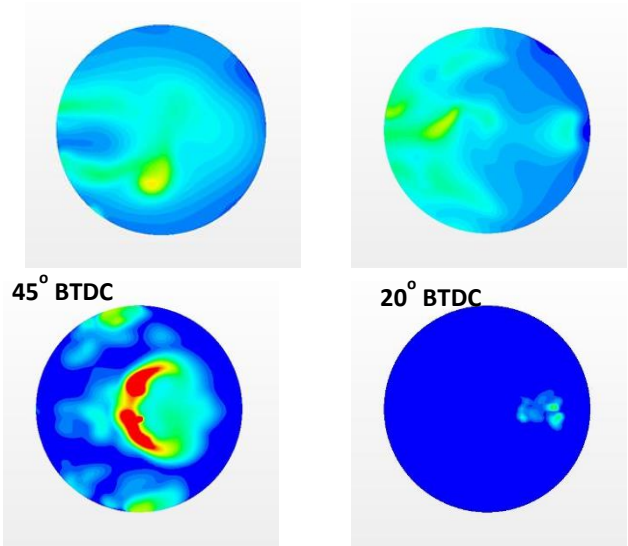

(a) Along Spark Plug Cross-section

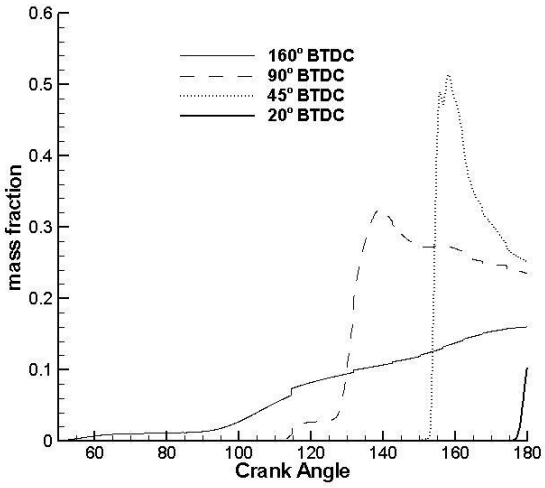

(b) Vapour Mass Fraction Time History

Figure 4. MASS FRACTION OF VAPOUR FOR DIFFERENT START OF INJECTION

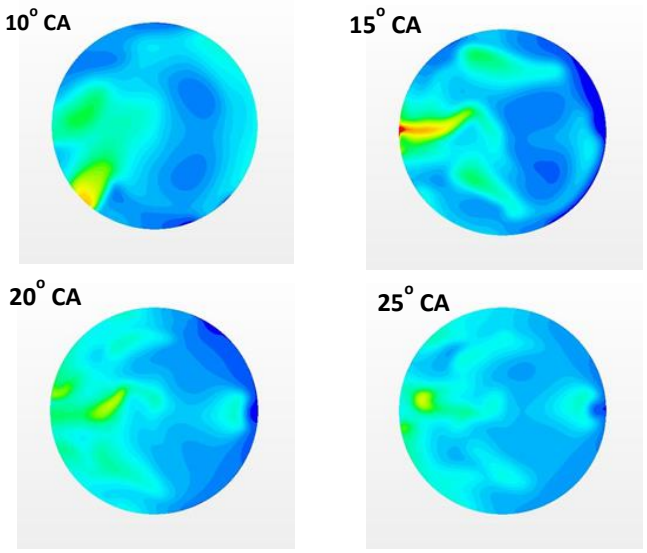

(a) Along Spark Plug Cross-section

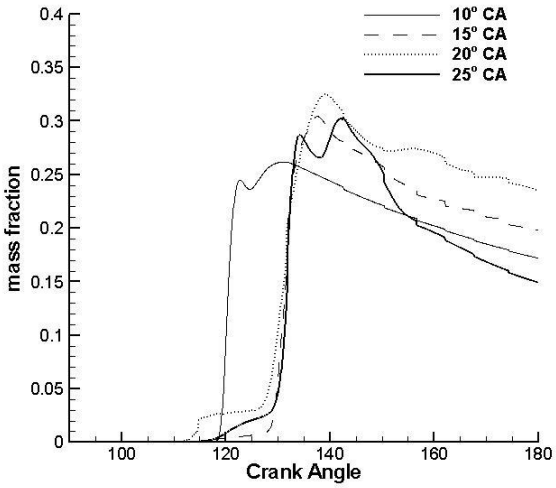

(b) Vapour Mass Fraction Time History

Figure 5. MASS FRACTION OF VAPOUR FOR DIFFERENT INJECTION LENGTH

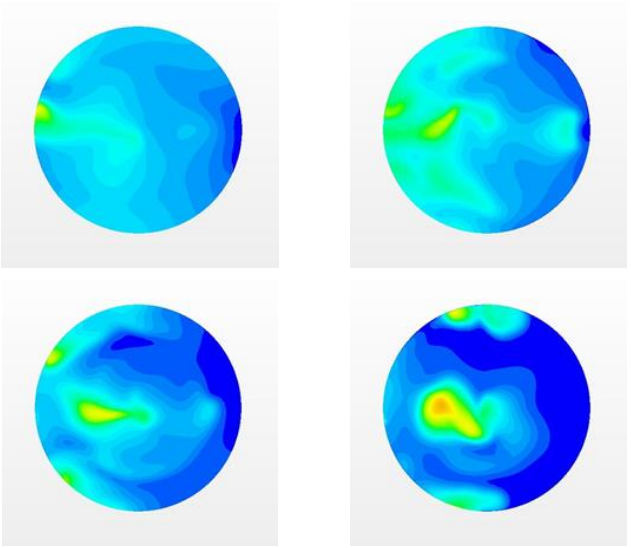

(a) Along Spark Plug Cross-section

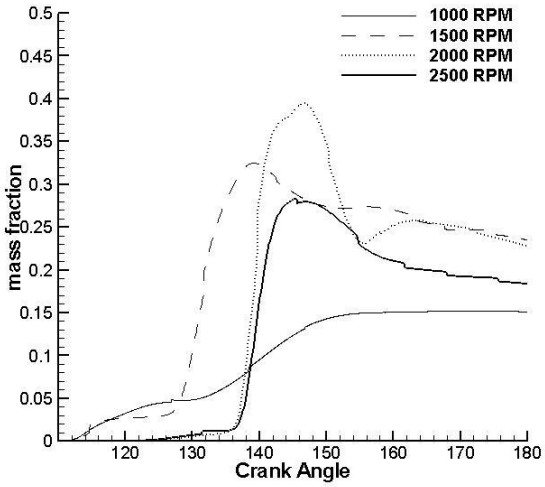

(b) Vapour Mass Fraction Time History

Figure 6. MASS FRACTION OF VAPOUR FOR ENGINE RPM